

obtaining the stopping- K^- exposure. We are very grateful to the Nevis scanning and measuring staffs

and their supervisors for their painstaking efforts which made this measurement possible.

*Research supported by the U. S. Atomic Energy Commission.

†Present address: University of California, Berkeley, California.

¹A. A. Belavin and I. M. Narodetsky, *Phys. Letters* **26B**, 668 (1968).

²W. E. Humphrey and R. R. Ross, *Phys. Rev.* **127**, 1305 (1962).

³J. A. Anderson *et al.*, in *Proceedings of the 1962 Con-*

ference on High-Energy Physics at CERN, edited by J. Prentki (CERN, Geneva, Switzerland, 1962), p. 832.

⁴D. Berley, Brookhaven National Laboratory AGS Department Internal Report No. 6/11/65 (unpublished).

⁵C. Baltay *et al.*, *Phys. Rev. Letters* **22**, 615 (1969).

⁶B. Sechi-Zorn *et al.*, *Phys. Rev.* **175**, 1735 (1968).

⁷G. Alexander *et al.*, *Phys. Rev.* **173**, 1452 (1968).

⁸Particle Data Group, *Rev. Mod. Phys.* **42**, 87 (1970).

PHYSICAL REVIEW D

VOLUME 4, NUMBER 3

1 AUGUST 1971

$\pi^+ p$ Elastic Scattering Data between 1820- and 2090-MeV c.m. Energy*

G. E. Kalmus, W. Michael, and R. W. Birge

Lawrence Radiation Laboratory, University of California, Berkeley, California 94720

and

S. Y. Fung and A. Kernan

University of California, Riverside, California 92502

(Received 18 September 1970)

Total and differential elastic cross-section data are presented at eight incident π^+ momenta: 1.28, 1.34, 1.40, 1.43, 1.55, 1.68, 1.77, and 1.84 GeV/c. These data were obtained from a hydrogen-bubble-chamber exposure at the Bevatron, and contain more than 65 000 events. This represents more than $1\frac{1}{2}$ times the world's data hitherto available in this energy region.

I. INTRODUCTION

We present total and differential cross sections for $\pi^+ p$ elastic scattering at eight incident π^+ momenta: 1.28, 1.34, 1.40, 1.43, 1.55, 1.68, 1.77, and 1.84 GeV/c. These data, byproducts of an extensive investigation of inelastic $\pi^+ p$ scattering, represent more than 1.5 times the world's differential cross-section data, up to now, in this energy region.¹⁻⁶ They result from the measurement of about 230 000 "two-prong" interactions in the Lawrence Radiation Laboratory 72- and 25-in. bubble chambers. The range in the cosine of the production angle covered by the data is $-1.0 < \cos \theta^*$

< 0.98 at the six higher momenta, and $-1.0 < \cos \theta^* < 0.96$ at the two lower momenta, where θ^* is the angle in the c.m. system between the pion in the final state and the beam direction.

II. EXPERIMENTAL PROCEDURE

A. Beam

The π^+ beam used for the three momenta in the 72-in. chamber (1.34, 1.43, and 1.68 GeV/c) had a single stage of separation with two vertical slits, the second being used to clean up the beam close to the bubble chamber. The momentum bite of the beam was $< \pm 1\%$. The proton contamination of the

beam was negligible, and the μ^+ contamination was estimated to be $(5 \pm 3)\%$. The beam used for the five momenta in the 25-in. chamber was the K67 beam, which had two stages of separation. The momentum bite was $< \pm 1\%$, the proton contamination was negligible, and the μ^+ contamination was estimated to be $(3 \pm 2)\%$.

B. Scanning and Measuring

The film was scanned for two-pronged events and roads were made for the Lawrence Radiation Laboratory Flying-Spot Digitizer (FSD) in a single pass. Approximately 10% of the film was re-scanned to obtain an over-all scanning efficiency. Events with a short proton (< 2 -cm projected length in space) were measured by using the "crutch point" mode. In this, the scanner digitizes, on the roadmaker, the end of the proton track as well as the vertex point in each view. These points are transferred directly into the geometry program where a vector in space is reconstructed by using these points. The magnitude and direction of this vector (and their errors) are used in the fitting program. For proton track lengths of > 1.5 cm projected (≈ 1 mm on film) it has been shown that the FSD has a constant (and high) efficiency. At five of the eight momenta all events that failed to get through the geometry program (FOG) were re-measured. These remeasurements were used to determine whether these events were biased. It was found that these events were consistent in angular distribution with those that went through on the first pass. However, both passes showed a small but measurable (with high statistics) bias against low-momentum backward pions, which were also close in azimuth to the plane containing the optical axis and the beam direction. (This is further discussed in Sec. III B.) The measuring efficiency (defined as the number of events that pass

geometry) divided by the number of events that had roads made was between 85% and 90% for each pass, except for a small number of rolls in which, because of bad film (edge marks missing or light tracks), it was lower than this. The three momenta that were not remeasured were, in fact, on the high side of this range. The fact that the remeasurements are essentially unbiased is not surprising when the usual reasons for failure are examined. These are predominantly overlapping beam tracks, confused origins, and tracks going outside their roads — the last of which is usually due to badly measured fiducials (on the roadmaker).

In addition to the main scanning and measuring of the data, a subset of data was handled somewhat differently in order to obtain the total elastic cross section. This is described in Sec. III B.

Table I gives the parameters of the exposure and the total elastic cross sections.

III. DATA

A. Geometry and Kinematics

All events measured were processed through the FOG-CLOUDY system of programs for reconstruction and kinematic fitting. The resulting kinematics, together with the ionization information obtained from the FSD, was then input into FAIR, where the assignment of a particular reaction (π^+p , $\pi^+p\pi^0$, $\pi^+p\eta^0$, $\pi^+\pi^+n$) was made on the basis of both the kinematic χ^2 and an ionization χ^2 . It was found that events that were kinematically ambiguous between a 4-constraint (4c) elastic hypothesis and any of the 1c hypotheses were, in fact, always elastic scattering. This left only the small number of events that were ambiguous between $\pi^+p \rightarrow \pi^+p$ and $\pi^+p \rightarrow p\pi^+$, i.e., for which a good fit was obtained when either track was assumed to be a pion (and the other a proton). These events, which occur when the lab momenta (and, therefore, the

TABLE I. Parameters of the exposure and cross sections.

Beam momentum (GeV/c)	Total c.m. energy (GeV)	Number of two-prong events measured	N_t Number of events within the accepted range in $\cos\theta^*$ and ϕ	N Number of events under the fitted curve $-1 < \cos\theta^* < 1$	Cross section (mb)
1.28	1.820	13 000	3730	4428	15.5 ± 1.1
1.34	1.850	39 000	9627	11 981	17.5 ± 1.2
1.40	1.880	21 000	6849	7891	17.1 ± 1.2
1.43	1.890	31 000	8357	10 327	20.7 ± 1.5
1.55	1.950	40 000	13 274	16 001	15.2 ± 1.0
1.68	2.010	37 000	8319	10 543	13.6 ± 1.0
1.77	2.060	24 000	9580	11 550	11.6 ± 0.8
1.84	2.090	25 000	6644	8031	9.9 ± 0.7

lab angles) of the two outgoing tracks are the same, were resolved by means of the ionization measurements. It should be noted that although these events populate a single region in angular distribution, it is the same for either mass hypothesis, and so even if the wrong hypothesis is used, no distortion of the angular distribution results.

B. Weighting of Events

Two biases are known to be present in the data.

(1) In events with a small momentum transfer to the proton, the recoil proton is often so small as to be undetectable. Below about $P_p = 100$ MeV/c (3 mm in space) the scanning efficiency is very small. Between 100 MeV/c and about 250 MeV/c (7 cm in space) the scanning efficiency was found to depend on the azimuthal angle of the proton. This effect is illustrated clearly in Fig. 1. This shows a scatter plot of $\cos\theta^*$ versus ϕ , the azimuth of the proton around the beam direction. The zero in ϕ is defined as being in the plane containing the beam direction and the optic axis of the camera. Figure 1 shows this plot at one of our momenta (1.43 GeV/c) and for $0.9 < \cos\theta^* < 1.0$. The depletion of events around $\phi = 0^\circ$, 180° , and 360° is clearly seen, as is the fact that as $\cos\theta^*$ decreases (and P_p increases) so the bias decreases. Since the $\cos\theta^*$ distribution should not depend on ϕ , we have used only part of the ϕ range for $0.9 < \cos\theta^* < 1.0$. To determine how much of the ϕ range to use, projections of the kind shown in Figs. 2(a) through 2(d) were used. These histograms show the projections of the plot in Fig. 1 onto the ϕ axis for the regions of $\cos\theta^*$ 0.98 to

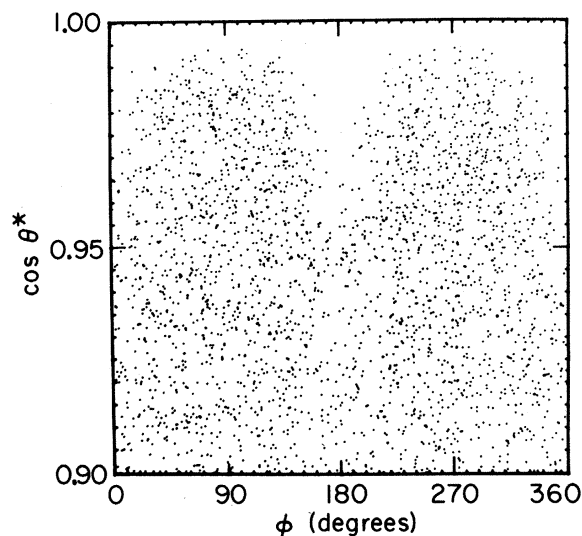


FIG. 1. Scatter plot of ϕ versus $\cos\theta^*$ at 1.43 GeV/c for forward scattering angles ($0.9 < \cos\theta^* < 1.0$).

0.96, 0.96 to 0.94, 0.94 to 0.92, and 0.92 to 0.90. An unbiased ϕ plot should be flat; this is a necessary but not sufficient condition. It is also necessary to establish that no events are missed uniformly in the flat region of histograms. This was checked by the rescanning, where no bias towards protons of projected length > 7 mm in space (6 mm on scan table) was found. The maximum convenient values of $\cos\theta^*$ which gave at least half the ϕ range (90 ± 45 deg and 270 ± 45 deg) with the above conditions were $\cos\theta^* = 0.96$ for our two lower momenta (1.28 and 1.34 GeV/c) and $\cos\theta^* = 0.98$ for the higher momenta. Clearly, as the beam momentum increases or $\cos\theta^*$ decreases (and the proton momentum increases), so the usable portion of ϕ increases.

(2) A small bias in the data also exists in the backward direction, i.e., for $-1.0 < \cos\theta^* < -0.95$. This can be seen in Fig. 3, which is a histogram of ϕ for the region $-1.0 < \cos\theta^* < -0.95$ at 1.55 GeV/c. The events missing have backward pions (in both the c.m. and lab frames) which, when combined with a ϕ of close to 0 or 180° , lie right on top of the beam track near the vertex, and therefore have a slightly higher-than-normal failure rate.

IV. RESULTS

A. Total Elastic Cross Sections

The total elastic cross sections were obtained in the following way:

(1) A sample of film at each momentum containing between 400 and 800 accepted elastic events was carefully rescanned.

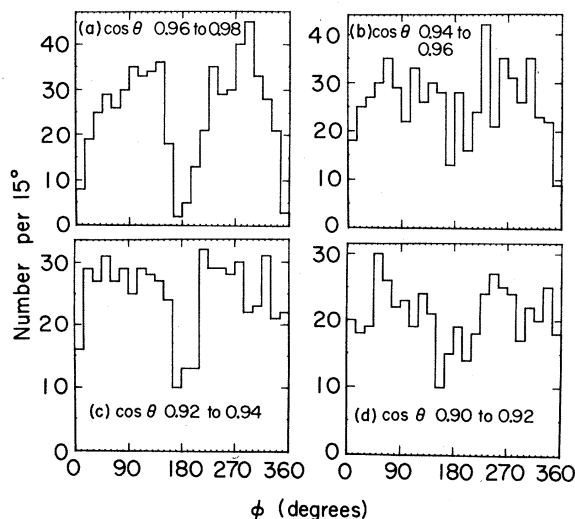


FIG. 2. Histograms of ϕ for various regions of $\cos\theta^*$ at 1.43 GeV/c.

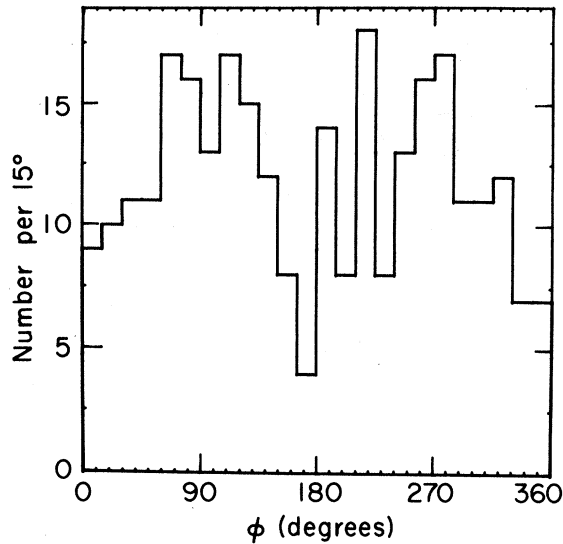


FIG. 3. Histogram of ϕ for $-1.00 < \cos \theta^* < -0.95$, i.e., the backward direction, at $1.55 \text{ GeV}/c$.

(2) Beam tracks were counted every 20 frames on the 25-in. chamber film (every 10 frames on 72-in. film) for these rolls. From this total we calculated the π^+ path length (L) in these rolls, taking into account the loss of beam due to interactions (based on the known π^+ total cross section) and the μ^+ contamination.

(3) All two-prongs found in the first scan were traced through the FSD (HAZE), geometry (FOG), kinematics (CLOUDY), and library (FAIR) programs in order to determine the throughput efficiency of the system.

(4) About 150 events at each momentum, from the above sample of film, that were within the fiducial volume but failed to fit any of the hypotheses π^+p , $p\pi^+$, $\pi^+p\pi^0$, $p\pi^+\pi^0$, $\pi^+\pi^+n$, $\pi^+p\eta$, or $p\pi^+\eta$ with a satisfactory χ^2 , were remeasured in order to determine the measuring efficiency for events that go through geometry.

We now define the following quantities for the sample of film at each momentum:

N_f , the number of accepted elastic events in the sample of film;

L , the total π^+ path length taking into account the μ^+ contamination and beam loss due to interactions (based on the known total cross sections);

ϵ_1 , the scanning efficiency of the first scan;

ϵ_2 , the throughput efficiency of the system;

ϵ_3 , the measuring efficiency for elastic events.

(It should be noted that the way in which ϵ_3 was measured ensured that ϵ_3 included both the effect of bad first measures and the effect of the tail of the first-measure χ^2 distribution.)

The total number of elastic scatters (N_T) in the sample of film at each momentum is given by

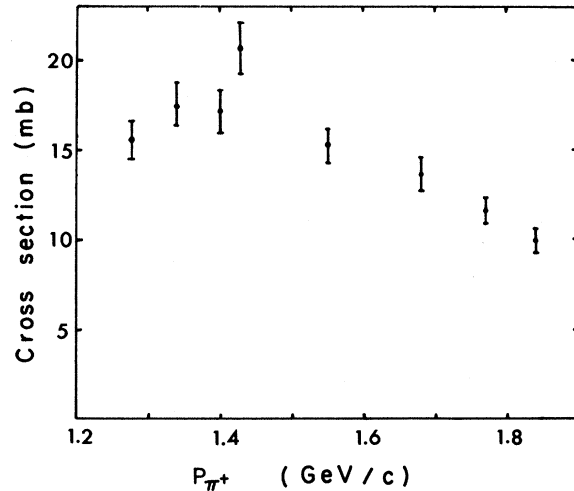


FIG. 4. Plot of total elastic cross section.

$$N_T = N_f \left(\frac{1}{\epsilon_1} \times \frac{1}{\epsilon_2} \times \frac{1}{\epsilon_3} \right) \times \frac{N}{N_f},$$

where N_f is the total number of elastic events accepted in the entire film (at one momentum) and N is the area under the fitted Legendre polynomial (see Sec. IV B).

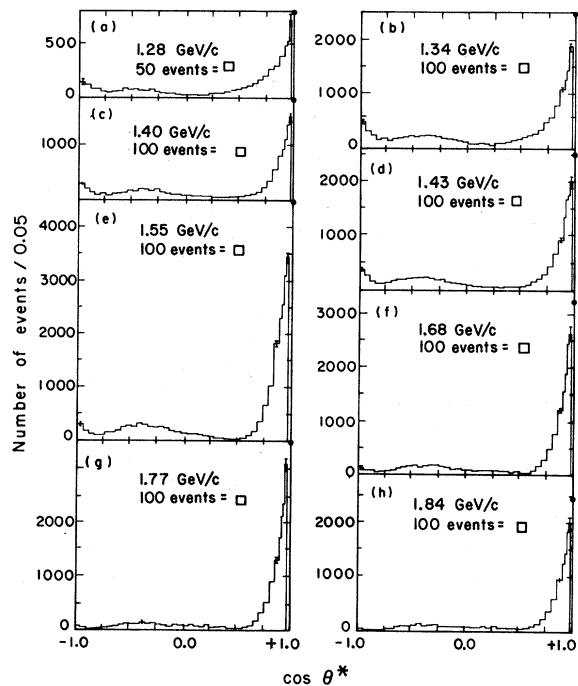


FIG. 5. Angular distributions. The dot on the ordinate at $\cos \theta^* = 1$ is the point obtained from the extrapolation using the Legendre series. The events in the histogram are weighted. Typical errors are shown on some of the boxes. For the cross sections, see Table II.

TABLE II. Differential cross sections and errors.

cos θ^* interval	1.28 GeV/c		1.34 GeV/c		1.40 GeV/c		1.43 GeV/c	
	Cross section (mb/sr)	Error in cross section (mb/sr)						
-1.00 -0.95	1.515	0.130	2.213	0.105	1.842	0.113	2.208	0.127
-0.95 -0.90	1.259	0.118	1.404	0.081	1.249	0.093	1.544	0.099
-0.90 -0.85	0.847	0.097	1.032	0.069	0.869	0.077	0.874	0.075
-0.85 -0.80	0.813	0.095	0.670	0.056	0.545	0.061	0.632	0.063
-0.80 -0.75	0.646	0.085	0.730	0.058	0.752	0.072	0.676	0.066
-0.75 -0.70	0.535	0.077	0.581	0.052	0.648	0.067	0.721	0.068
-0.70 -0.65	0.591	0.081	0.758	0.059	0.793	0.074	0.944	0.078
-0.65 -0.60	0.635	0.084	0.786	0.060	0.786	0.074	1.117	0.084
-0.60 -0.55	0.925	0.102	0.911	0.065	0.821	0.075	1.129	0.085
-0.55 -0.50	0.747	0.091	0.981	0.068	1.069	0.086	1.251	0.089
-0.50 -0.45	0.780	0.093	0.921	0.065	0.973	0.082	1.353	0.093
-0.45 -0.40	0.802	0.095	0.995	0.068	1.262	0.093	1.365	0.093
-0.40 -0.35	0.780	0.093	1.032	0.069	1.207	0.091	1.397	0.094
-0.35 -0.30	0.802	0.095	0.967	0.067	1.090	0.087	1.244	0.089
-0.30 -0.25	0.613	0.083	0.907	0.065	1.152	0.089	1.142	0.085
-0.25 -0.20	0.466	0.070	0.767	0.060	0.869	0.077	1.187	0.087
-0.20 -0.15	0.390	0.066	0.707	0.057	0.731	0.071	0.880	0.075
-0.15 -0.10	0.435	0.070	0.637	0.054	0.573	0.063	0.804	0.072
-0.10 -0.05	0.301	0.058	0.530	0.050	0.579	0.063	0.721	0.068
-0.05 0.00	0.256	0.053	0.446	0.046	0.462	0.056	0.555	0.060
0.00 0.05	0.279	0.056	0.260	0.035	0.483	0.058	0.523	0.058
0.05 0.10	0.267	0.055	0.242	0.034	0.345	0.049	0.396	0.050
0.10 0.15	0.223	0.050	0.284	0.036	0.331	0.048	0.357	0.048
0.15 0.20	0.167	0.043	0.251	0.034	0.269	0.043	0.287	0.043
0.20 0.25	0.334	0.061	0.135	0.025	0.297	0.045	0.287	0.043
0.25 0.30	0.412	0.068	0.335	0.039	0.248	0.041	0.274	0.042
0.30 0.35	0.379	0.065	0.344	0.040	0.214	0.038	0.230	0.038
0.35 0.40	0.479	0.073	0.442	0.045	0.255	0.042	0.332	0.046
0.40 0.45	0.691	0.088	0.553	0.051	0.283	0.044	0.313	0.045
0.45 0.50	0.780	0.093	0.637	0.054	0.276	0.044	0.319	0.045
0.50 0.55	0.936	0.102	0.837	0.062	0.304	0.046	0.357	0.048
0.55 0.60	1.103	0.111	1.009	0.068	0.476	0.057	0.549	0.059
0.60 0.65	1.393	0.125	1.181	0.074	0.621	0.065	0.938	0.077
0.65 0.70	1.760	0.140	1.497	0.083	0.821	0.075	1.231	0.089
0.70 0.75	2.128	0.154	2.092	0.099	1.449	0.100	1.793	0.107
0.75 0.80	2.819	0.177	2.571	0.109	2.228	0.124	2.744	0.132
0.80 0.85	3.209	0.189	3.580	0.129	3.552	0.157	4.294	0.166
0.85 0.90	4.223	0.217	5.035	0.153	5.442	0.194	5.934	0.195
0.90 0.92	5.376	0.424	5.823	0.319	6.329	0.330	8.629	0.454
0.92 0.94	5.822	0.447	6.660	0.341	7.657	0.399	10.703	0.506
0.94 0.96	8.078	0.581	8.683	0.389	9.536	0.444	11.229	0.519
0.96 0.98	10.605	0.524	12.729	0.637

The total elastic cross section is given by

$$\sigma_{e1} = (27\,800/L) \times N_T \text{ mb,}$$

where L is in cm (at the operating conditions of the chamber 1 mb is equivalent to 27 800 cm of path length).

The error in σ_{e1} has been calculated by combining the following effects:

- (a) Statistical error in $N_f \approx 5\%$.
- (b) Statistical error in number of beam tracks counted $\approx 2.5\%$.
- (c) Error in μ contamination $\approx 2\%$.
- (d) Error in $\epsilon_1 \approx 2\%$.
- (e) Error in $\epsilon_2 \approx 1\%$.
- (f) Error in $\epsilon_3 \approx 2\%$.
- (g) Error in $N_f \approx 1\%$.
- (h) Error in $N \approx 1\%$.

TABLE II (Continued)

		1.55 GeV/c		1.68 GeV/c		1.77 GeV/c		1.84 GeV/c	
$\cos\theta^*$ interval		Cross section (mb/sr)	Error in cross section (mb/sr)						
-1.00	-0.95	0.978	0.058	0.489	0.046	0.210	0.026	0.115	0.021
-0.95	-0.90	0.565	0.042	0.300	0.035	0.149	0.021	0.060	0.015
-0.90	-0.85	0.407	0.034	0.275	0.034	0.070	0.014	0.075	0.017
-0.85	-0.80	0.355	0.032	0.168	0.026	0.108	0.018	0.052	0.014
-0.80	-0.75	0.363	0.032	0.218	0.030	0.111	0.018	0.082	0.017
-0.75	-0.70	0.505	0.038	0.250	0.032	0.190	0.024	0.119	0.021
-0.70	-0.65	0.485	0.037	0.308	0.036	0.216	0.025	0.115	0.021
-0.65	-0.60	0.603	0.042	0.480	0.044	0.248	0.027	0.168	0.025
-0.60	-0.55	0.776	0.047	0.558	0.048	0.318	0.030	0.261	0.031
-0.55	-0.50	0.860	0.050	0.645	0.051	0.391	0.034	0.246	0.030
-0.50	-0.45	0.793	0.048	0.686	0.053	0.371	0.033	0.294	0.033
-0.45	-0.40	0.975	0.053	0.567	0.048	0.377	0.033	0.406	0.039
-0.40	-0.35	0.926	0.052	0.624	0.051	0.488	0.038	0.298	0.033
-0.35	-0.30	0.790	0.048	0.710	0.054	0.371	0.033	0.335	0.035
-0.30	-0.25	0.747	0.046	0.719	0.054	0.415	0.035	0.369	0.037
-0.25	-0.20	0.776	0.047	0.624	0.051	0.351	0.032	0.272	0.032
-0.20	-0.15	0.707	0.045	0.571	0.048	0.310	0.030	0.253	0.031
-0.15	-0.10	0.571	0.041	0.411	0.041	0.254	0.027	0.264	0.031
-0.10	-0.05	0.505	0.038	0.468	0.044	0.351	0.032	0.027	0.032
-0.05	0.00	0.421	0.035	0.337	0.037	0.310	0.030	0.276	0.032
0.00	0.05	0.407	0.034	0.431	0.042	0.298	0.030	0.268	0.032
0.05	0.10	0.398	0.034	0.283	0.034	0.342	0.032	0.272	0.032
0.10	0.15	0.369	0.033	0.324	0.036	0.289	0.029	0.250	0.030
0.15	0.20	0.323	0.031	0.300	0.035	0.257	0.027	0.276	0.032
0.20	0.25	0.251	0.027	0.316	0.036	0.351	0.032	0.242	0.030
0.25	0.30	0.231	0.026	0.333	0.037	0.216	0.025	0.365	0.037
0.30	0.35	0.153	0.021	0.242	0.032	0.242	0.027	0.227	0.029
0.35	0.40	0.141	0.020	0.242	0.032	0.257	0.027	0.246	0.030
0.40	0.45	0.104	0.017	0.160	0.026	0.166	0.022	0.190	0.027
0.45	0.50	0.098	0.017	0.197	0.028	0.166	0.022	0.194	0.272
0.50	0.55	0.101	0.017	0.140	0.024	0.166	0.022	0.171	0.025
0.55	0.60	0.164	0.022	0.172	0.027	0.275	0.028	0.250	0.030
0.60	0.65	0.297	0.029	0.300	0.035	0.336	0.031	0.395	0.038
0.65	0.70	0.554	0.040	0.616	0.050	0.584	0.041	0.577	0.046
0.70	0.75	1.093	0.056	1.158	0.069	1.046	0.055	0.931	0.059
0.75	0.80	1.953	0.075	1.979	0.090	1.653	0.069	1.464	0.074
0.80	0.85	3.029	0.093	3.096	0.113	2.787	0.090	2.347	0.094
0.85	0.90	5.325	0.124	4.952	0.143	3.987	0.108	3.695	0.117
0.90	0.92	6.699	0.241	6.405	0.281	5.156	0.194	4.806	0.212
0.92	0.94	7.449	0.254	7.719	0.308	6.397	0.237	5.467	0.247
0.94	0.96	9.014	0.279	9.998	0.392	6.952	0.247	6.957	0.279
0.96	0.98	10.038	0.330	10.778	0.470	9.201	0.317	7.478	0.323

The last of these was estimated by increasing the order of fit by one and seeing how much the area under the curve changed, as well as by the usual propagation of errors.

Thus it can be seen that the statistical error in N_p , and the other errors combined, contribute equally to the final error of $\approx 7\%$.

Table I and Fig. 4 show the elastic cross sections obtained.

B. Angular Distributions

Table II and Fig. 5 show the angular distributions at the various momenta. In Fig. 5 the histograms of weighted events have been plotted in such a way that equal areas correspond to equal numbers of events, since the bin size above $\cos\theta^* = 0.90$ has been decreased. These data, in the bins shown, were then fitted with a Legendre series, using a

TABLE III. Legendre shape coefficients.

P_{π^+} (GeV/c)	1.28	1.34	1.40	1.43	1.55	1.68	1.77	1.84
A_1/A_0	1.185 ± 0.050	1.099 ± 0.031	1.127 ± 0.032	1.153 ± 0.030	1.406 ± 0.023	1.696 ± 0.031	1.878 ± 0.028	1.961 ± 0.033
A_2/A_0	1.961 ± 0.072	2.019 ± 0.045	2.112 ± 0.046	2.124 ± 0.044	2.245 ± 0.034	2.375 ± 0.045	2.425 ± 0.041	2.428 ± 0.049
A_3/A_0	1.367 ± 0.088	1.613 ± 0.055	2.124 ± 0.055	2.146 ± 0.053	2.615 ± 0.040	2.787 ± 0.054	2.741 ± 0.048	2.729 ± 0.058
A_4/A_0	0.926 ± 0.102	1.298 ± 0.063	1.733 ± 0.061	1.728 ± 0.059	2.062 ± 0.044	2.212 ± 0.059	2.161 ± 0.053	2.178 ± 0.063
A_5/A_0	0.234 ± 0.105	0.293 ± 0.063	0.616 ± 0.062	0.584 ± 0.059	0.974 ± 0.043	1.215 ± 0.057	1.257 ± 0.052	1.301 ± 0.063
A_6/A_0	0.533 ± 0.101	0.768 ± 0.061	0.816 ± 0.059	0.877 ± 0.055	0.855 ± 0.039	0.895 ± 0.052	0.766 ± 0.048	0.762 ± 0.058
A_7/A_0	0.104 ± 0.081	0.201 ± 0.048	0.105 ± 0.050	0.096 ± 0.045	0.108 ± 0.033	0.170 ± 0.044	0.111 ± 0.042	0.157 ± 0.051
A_8/A_0	-0.013 ± 0.073	0.074 ± 0.044	-0.049 ± 0.049	0.045 ± 0.044	-0.013 ± 0.032	-0.085 ± 0.038	-0.025 ± 0.033	-0.060 ± 0.038
χ^2	31	43	37	28	45	44	56	35
D. F. ^a	33	33	34	34	34	34	34	34

^aNumber of degrees of freedom.

least-squares method, in the range $-1.0 < \cos \theta^* < 0.98$ for the six higher momenta and $-1.0 < \cos \theta^* < 0.96$ for the two lower momenta. The expansion used was

$$\frac{dN}{d(\cos \theta^*)} = \frac{1}{2} \sum_{n=0}^8 A_n P_n(\cos \theta^*).$$

Table III gives the values of coefficients of the Legendre series normalized to the zeroth order, A_1/A_0 up to A_8/A_0 . At no momentum was a higher order needed to fit the data. A typical curve of χ^2 divided by the number of degrees of freedom is shown in Fig. 6. The area under the fitted Legendre curve is proportional to the total number $N(=A_0)$ of elastic events (at all angles).

The differential cross sections in mb/sr given in Table II are directly proportional to the number of events per unit interval in $\cos \theta^*$. Strictly speaking, they should be interpreted as a mean for each bin, but since the forward bins have been split into fine intervals, a very good approximation is to use the midpoint of each bin.

The constant of proportionality is given by

$$\left. \frac{d\sigma}{d\Omega} \right|_{\text{averaged over bin } i} = \frac{N_i}{N} \times \sigma_{el} \times \frac{1}{\Delta \cos \theta_i^*} \frac{1}{2\pi},$$

where N_i is the number of events in bin i (or weighted number), and $\Delta \cos \theta_i^*$ is the bin width.

The error in σ_{el} has *not* been propagated into $d\sigma/d\Omega$, since it affects only the over-all normalization and not the relative error between bins.

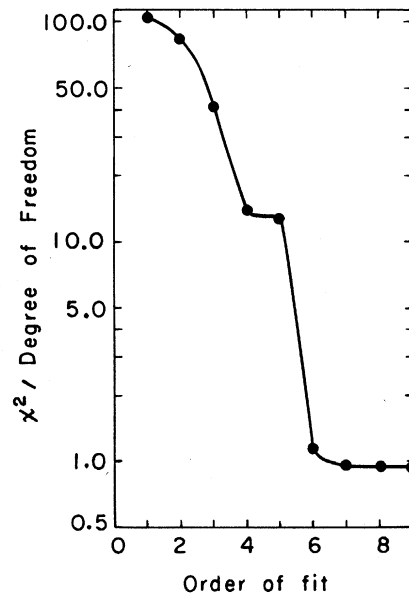


FIG. 6. Curve of χ^2 divided by the number of degrees of freedom as a function of the order of fit for 1.43 GeV/c.

V. DISCUSSION

The purpose of this paper is to present our data in such a form that they may readily be used in phase-shift analyses. The differential cross sections are of precision comparable to or greater than others in the literature in this energy region, and have greater range in $\cos\theta^*$. The Legendre shape coefficients (Table III) are in good agreement with those of Duke *et al.*,⁴ and Busza *et al.*,² in the energy region common to those experiments. The coefficients from this experiment have significantly smaller error due to the greater range of $\cos\theta^*$. The total elastic cross sections presented are also in good agreement with those in the literature (see Fig. 4) with the possible exception of our point at 1.55 GeV/c. The general method used to determine the total elastic cross section was also the one used to determine the various inelas-

tic-channel cross sections, for which it is more appropriate. In this method it is very difficult to determine systematic effects to within less than 4 or 5 percent, and therefore we decided to match our statistical error to this.

ACKNOWLEDGMENTS

We thank Howard White, Dennis Hall, and Loren Shaltz of the Data Handling Group for their efforts in processing the data, and we are grateful to the scanners and measurers of the Powell-Birge group, particularly, Toni Woodford, who did much of the work necessary in determining the total elastic cross sections. Finally, we acknowledge the efforts of Bert Albrecht, John Visser, Charlotte Scales, and Maggie Morley, who were involved in the all-important bookkeeping aspects of this experiment.

*Work done under the auspices of the U. S. Atomic Energy Commission.

¹W. Busza *et al.*, Phys. Rev. 180, 1339 (1969).

²V. Cook *et al.*, Phys. Rev. 130, 761 (1963).

³A. Daudin *et al.*, Nuovo Cimento 33, 1300 (1964).

⁴P. J. Duke *et al.*, Phys. Rev. Letters 15, 468 (1965);

Rutherford High-Energy Laboratory Report No. RHEL-M128, 1967 (unpublished).

⁵J. A. Helland *et al.*, Phys. Rev. 134, B1062 (1967).

⁶G. Giacomelli, P. Pini, and S. Stagni, CERN Report No. CERN/HERA 69-1 (unpublished).